Communication

Distributions of Grain Boundary Normals in the Laboratory Reference Frame

KRZYSZTOF GLOWINSKI
and GREGORY S. ROHRER

Distributions of grain boundary normals with their components expressed in the laboratory reference frame are obtained for yttria and austenitic steel based on three-dimensional electron backscatter diffraction data. The distributions exhibit various extrema that are attributed to the inaccuracy of the boundary surface reconstruction and to the discrete nature of the orientation data. We provide interpretation of the distributions with particular emphasis put on indicating the sources of these artifacts. Moreover, we verify the negligible impact of these issues on grain boundary plane and character distributions.

DOI: 10.1007/s11661-016-3468-9

Currently available experimental techniques (*e.g.*, References 1–3) make it possible to acquire three-dimensional (3D) orientation maps of polycrystals containing several thousand grains; see, *e.g.*, References 4 and 5. From such maps, the surfaces of boundaries separating abutting grains (and vectors normal to these surfaces) can be extracted along with the misorientations of the crystal lattices of the adjacent grains. Thus, all five so-called macroscopic boundary parameters are accessible. It is well known that grain boundaries have a strong impact on the properties of materials, and owing to the significant sizes of the boundary datasets which are being collected, statistical analysis of boundary networks incorporating both the misorientations and the normals has become an important branch of (3D) materials science. Grain boundaries can be studied from different points of view, and effective ways of gathering and representing boundary data are sought after. For instance, there is some interest in distributions of triple junctions,[6] but still the more common approach is computation of misorientation distribution functions,[7] grain boundary plane, and character distributions (GBPDs and GBCDs)[8,9] which depict populations of boundaries as functions of, respectively, grain misorientations, boundary normals, and all five parameters collectively. In the case of GBCDs and GBPDs, coordinates of vectors normal to boundaries are expressed in the coordinate frames attached to grains.

In this note, we consider—and add to the above list—the distributions of boundary normals given in the laboratory reference frame. In order to distinguish them from GBPDs, they will be referred to as grain boundary inclination distributions (GBIDs). Functions of boundary normals in the sample frame were considered before;[10] however, their values were estimated using stereological methods. In what follows, an approach to computing GBIDs directly from 3D boundary data is described. It is then used for calculating GBIDs for yttria[4] and fully austenitic steel[5] samples. The obtained distributions contain artifacts revealing numerous distortions introduced to boundary networks during their reconstruction from the orientation maps. These distortions are enumerated, and suggestions for interpretation of GBIDs are given. (In a sense, this study is complementary to works devoted to the analysis of experimental biases occurring in 3D data collection, *e.g.*, Reference 11.) Eventually, the influence of the imperfections of boundary reconstruction on GBCDs and GBPDs is investigated. This is of particular importance as a number of GBCDs and GBPDs have already been published (*e.g.*, References 4 and 5).

The aforementioned 3D data of yttria and austenite (which are available for download at Reference 12) were registered in a dual-beam scanning electron microscope using the 3D electron backscatter diffraction technique (EBSD), *i.e.*, 2D orientation maps were acquired alternately with removal of layers of the material *via* ion milling.

The details of the materials and experimental setups can be found in References 4 and 5. It is worth mentioning that for Y_2O_3, the in-plane resolution was 0.07 μm and the thickness of each removed layer was 0.28 μm. For γ-Fe, these parameters were 0.15 and 0.2 μm, respectively. The average grain diameters for both materials were about 2.5 μm. The raw 3D-EBSD data were aligned and cleaned-up using the *DREAM.3D* package.[13] In the clean-up process, to all voxels whose crystal orientations were not reliable, the orientations of their high-quality immediate neighbors were iteratively assigned. Then, grains were reconstructed from groups of voxels having orientations differing by no more than 5 deg from one another. In the case of Y_2O_3, it was required that a grain is composed of at least 60 voxels, while for γ-Fe, 20 voxels were required. The orientation maps of yttria and austenite had the dimensions of

KRZYSZTOF GLOWINSKI, Visiting Scholar, and GREGORY S. ROHRER, W.W. Mullins Professor and Head, are with the Department of Materials Science and Engineering, Carnegie Mellon University, 5000 Forbes Ave., Pittsburgh, PA 15213-3890. Contact e-mail: kglowinski@ymail.com

Manuscript submitted December 17, 2015.
Article published online April 4, 2016

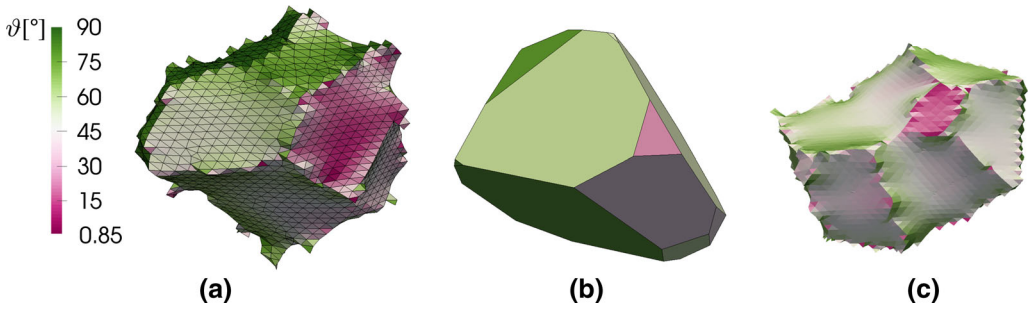

Fig. 1—(*a*) Grain boundaries (of one grain) extracted from 3D-EBSD data acquired from yttria. (*b*) Polyhedral grain taken from (exact) Voronoi tessellation. (*c*) Grain reconstructed from discrete approximation of Voronoi tesselation. Mesh segments (a, c) and facets (b) are colored according to the angle ϑ between their normals and the z axis.

about $32 \times 29 \times 11$ and $64 \times 33 \times 32\,\mu m^3$, respectively, and contained in total 5860 and 4210 grains, respectively (including the grains cut by the outer surfaces of the samples). In the next step, surfaces of grain boundaries were reconstructed in the form of meshes of triangular segments (Figure 1(a)) using *QuickMesh* and *Laplacian Smoothing* filters of *DREAM.3D*. The control parameters of the latter were set to the typical values: *Iteration Steps* = 100, *Default Lambda* = 0.25, *Triple Line Lambda* = 0.2, and *QuadruplePointsLambda* = 0.15; the remaining parameters were set to 0, *i.e.*, vertices of the segments lying at the outer surfaces of the samples were not smoothed. Only the boundaries of the grains that were entirely contained in the images were taken into consideration in the analyses described below. There were 3513 and 2541 such grains in the yttria and austenite samples, respectively.

The method for computing the distributions of boundary normals with their components expressed in the laboratory frame was outlined in Reference 14. The idea is to probe the distribution for unit vectors whose end-points are evenly distributed on the sphere and to sum areas of mesh segments that have normals deviated by less than a specified limiting angle ρ from a given sampling vector.[9] In this work, the distributions were computed in the Cartesian coordinate frames that were aligned in directions defined by the microscope stage and the EBSD software, and in which the z axis corresponds to the direction of serial sectioning, while the x and y base vectors point along the longer and the shorter of the remaining two edges, respectively. The limiting angle ρ was set to 7 deg as this value is believed to be close to the experimental accuracy for determining boundary inclinations.[8,9] Each boundary segment can be equivalently described by two vectors differing by the choice of sense. To avoid this ambiguity, the normals are selected to have non-negative z components, and the distribution is probed in the upper hemisphere. At the end, the areas accumulated for each sampling vector are divided by $2 \times A_{\text{total}} \times A_{\text{cap}}$ with A_{total} standing for the total area of all segments and A_{cap} being the area of a spherical cap restricted by ρ. With this normalization, the distribution is expressed as multiples of the random distribution (MRD)—the units typically used for GBCDs and GBPDs. With these units, normals for which the values are less or greater than 1 MRD are recognized as under- and over-represented (compared to random data), respectively.

GBIDs computed for yttria and austenite using the above approach are presented in Figure 2(a). In both distributions, there occur maxima for directions coinciding with the coordinate frame axes. The highest intensities are about 2.2 MRD for Y_2O_3 and about 1.7 MRD for γ-Fe. However, the locations and heights of the peaks brought the question whether these maxima are true features of the GBIDs or artifacts. Yttria is a ceramic produced by cold isostatic pressing and sintering; its microstructure is composed of equiaxed grains and has very weak anisotropy [4]. Therefore, a function close to a uniform distribution with values at the level of 1 MRD is expected. All possible artifacts need to be enumerated and filtered out before drawing any conclusions based on the obtained GBID. In contrast, austenite was about 60 pct cold rolled and annealed for a short time. Because its recrystallized microstructure reveals the brass-type crystallographic texture,[5] it would not be surprising if the processing history was also reflected in the GBID. Still, without a complete understanding of possible artifacts, the interpretation of any GBID would be unreliable.

The magnitude of statistical fluctuations likely to occur in the GBIDs was estimated using test data generated using the QHull[15] package as Voronoi tessellations with the seeds being points randomly dispersed in space. Such simple models composed of polyhedral 'grains' (see Figure 1(b)) are frequently used to approximate the basic statistics of polycrystals[16] and are the starting point to more advanced simulations.[17] As the number of grains in the model increased, the corresponding GBIDs converged to a uniform function with the value of 1 MRD (Figure 3). For models having the same dimensions and the same total numbers of grains as the considered experimental datasets, the fluctuations were relatively large: the distribution values were contained in the range from about 0.6 to about 1.4 MRD (Figure 2(b)). Hence, peaks smaller than 1.4 MRD and valleys shallower than 0.6 MRD cannot be recognized as true features of the GBIDs calculated for yttria and austenite. In order to facilitate future

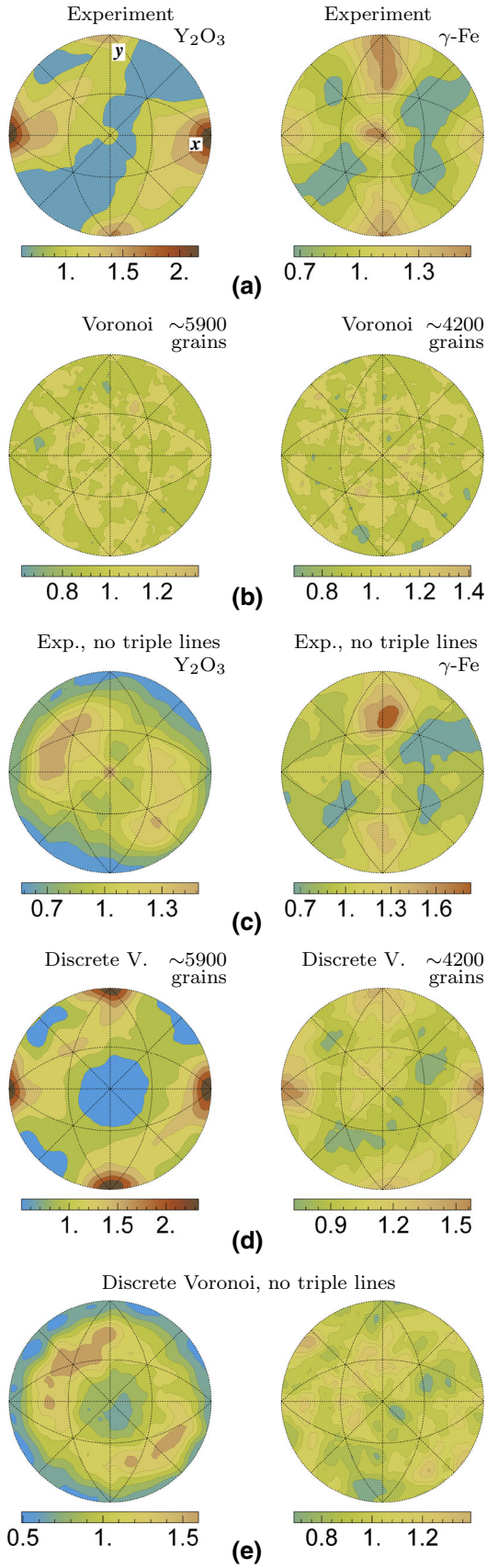

◀Fig. 2—Grain boundary inclination distributions obtained for: (*a*) experimental data, (*b*) (exact) Voronoi tessellations built of different numbers of polyhedral grains, (*c*) subsets of experimental data without mesh segments adjacent to triple lines, and for discrete approximations of Voronoi tessellations with triple lines (*d*) taken into account and (*e*) omitted. Distributions are plotted in stereographic projections. Intensities are given in MRDs.

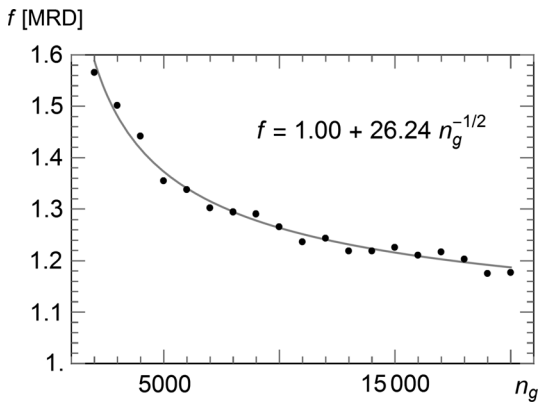

Fig. 3—Maximum values (*f*) observed in the grain boundary inclination distributions computed for (exact) Voronoi tessellations as a function of the total number of grains (n_g). To obtain this graph, multiple datasets for each value of n_g were analyzed; the synthetic microstructures had equal dimensions along all three axes.

analyses of GBIDs, the highest fluctuations observed for tessellations containing up to 20000 grains are collected in Figure 3.

It was noticed that the algorithms for smoothing grain boundary surfaces tend to leave stepped triple lines (Figure 1), especially if the voxels are not cubes, as in the case of yttria, where the in-plane resolution and the spacing between slices differ by a factor of 4. Therefore, GBIDs were also computed for subsets of the data with mesh segments directly neighboring triple lines excluded. By omitting these segments, the peaks for directions parallel to the *x* and *y* axes were eliminated (Figure 2(c)).

Implications of the discrete character of 3D-EBSD data were evaluated using different artificial datasets. Again, their dimensions and the numbers of grains they contained were adjusted to the experimental data. This time, however, instead of exact Voronoi tessellations, their discrete approximations were constructed using an in-house code. The voxel sizes were chosen to mimic the experimental resolutions. Random orientations were ascribed to grains in order to make it possible to process the test data using *DREAM.3D*. Afterward, surfaces of boundaries were reconstructed in the same way as in the case of the experimental data. It is apparent that after the typical smoothing, the grain shapes are not ideal polyhedra, and the triple lines remain uneven; see Figure 1(c). GBIDs computed for these datasets with segments adjacent to triple lines included and excluded are shown in Figures 2(d) and (e).

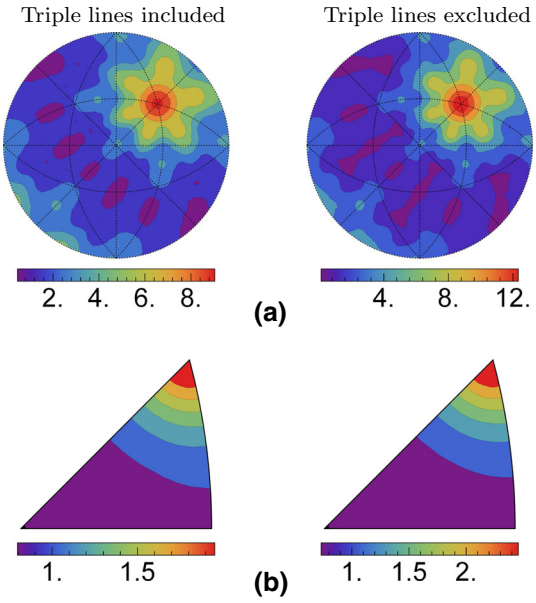

Fig. 4—Impact of exclusion of mesh segments directly neighboring triple lines (*a*) on the section for the misorientation of 60 deg about the [111] axis on the GBCD computed for yttria and (*b*) on GBPD obtained for austenite. The left- and right-hand side plots correspond to data with triple lines taken into consideration and ignored, respectively. GBCDs and GBPDs are expressed in MRDs and drawn in stereographic projections.

The elevated values for the $[\pm 1, 0, 0]$ and $[0, \pm 1, 0]$ normals are visible if there is a contribution from the 'triple lines,' while they are not seen when the triple lines are removed. Interestingly, there is no peak for the [0, 0, 1] vector for the test data corresponding to yttria (even if the triple lines are included in calculations), and for the austenite-like test data, the values near that direction are only slightly elevated; other tests indicate that with cubic voxels and 3D maps of equal dimensions in each direction, there may occur a significant peak also for the *z* direction.

Particularly interesting is the comparison of the experimental data of yttria with their synthetic counterpart. Besides a small peak for the [0, 0, 1] vector, all other maxima observed in the experimental data are also visible in the artificial data, disregarding whether the triple lines segments are considered or not. This leads to a conclusion that, besides the [0, 0, 1] peak, all other anisotropy is an artifact resulting from the discrete character (including the disproportion in voxel dimensions) and post-processing of the data. In the case of the test data which mimic the austenite sample, only random fluctuations are observed if the triple lines are neglected. Concluding, in the GBID obtained for austenite, only three peaks in the vicinities of the [0, 0, 1] and $[0, \pm 1, 1]/\sqrt{2}$ directions are not reproduced in the synthetic data.

For both experimental datasets, even when the triple lines are excluded, there are elevated values for the vector parallel to the *z* axis (Figure 2(a)). In 3D-EBSD data, the consecutive slices may be rotated, translated, or deformed; if these defects are not corrected, misfits between layers may lead to an excess of mesh segments lying in the *xy* plane, and thus, to peaks for the [0, 0, 1] vector in the GBID. To study the impact of this issue carefully, as well as the impact of the surface meshing technique and the smoothing parameters, more advanced simulations beyond the scope of the current letter would be needed.

Now, the question arises, how does the exclusion of the segments adjacent to triple lines affect the boundary distributions given in the crystallite frame. Example sections through GBCDs obtained for yttria (with and without removing the triple lines) and example GBPDs computed for austenite are presented in Figure 4. (The values of these distribution functions may be different compared to the functions published in References 4 and 5 because we used different computational methods[9,14] and different 'bin' sizes.) Since mesh segments directly neighboring triple lines may constitute as much as 40 pct of all segments (in the case of voxels having similar dimensions along three axes), the normalization factors may differ significantly. This explains the differences in heights of the peaks depending on whether the triple lines are taken into account or not. Nevertheless, in both cases, the locations of the maxima are the same and the relative heights of the peaks remain similar provided that the amount of data is large enough (*i.e.*, statistical fluctuations are relatively small). Even if there are mesh segments with similar inclinations in the laboratory frame, their normals are generally different in the crystal frame. These segments will be seen as an additional background in GBCDs and GBPDs unless there is a sharp texture in the material.

In summary, a method for computing distributions of boundary inclinations in the laboratory frame (abbreviated GBID) has been presented and demonstrated on two experimental datasets. The obtained distributions appear to be very sensitive to the imperfections of the reconstructed boundaries. For this reason, GBIDs can be utilized as a tool for evaluation of the performance of data post-processing algorithms and software. In order to interpret the experimental GBIDs correctly, it has been suggested to compare them to GBIDs obtained from dedicated computer-generated datasets. Finally, the impact of the distortions on the conclusions drawn from the GBCDs and GBPDs has been shown to be minor.

The authors would like to thank H. Beladi, S.J. Dillon, and N.T. Nuhfer for providing the 3D-EBSD data used in this work. K.G. received funds for his work from the National Science Center Poland based on DEC-2014/12/T/ST8/00086. G.S.R. acknowledges support from the National Science Foundation under MRI Grant DMR 1428480.

REFERENCES

1. M.P. Echlin, A. Mottura, C.J. Torbet, and T.M. Pollock: *Rev. Sci. Instrum.*, 2012, vol. 83, p. 023701.

2. U. Lienert, S.F. Li, C.M. Hefferan, J. Lind, R.M. Suter, J.V. Bernier, N.R. Barton, M.C. Brandes, M.J. Mills, M.P. Miller, B. Jakobsen, and W. Pantleon: *JOM*, 2011, vol. 63, pp. 70–77.
3. S. Peetermans, A. King, W. Ludwig, P. Reischig, and E.H. Lehmann: *Analyst*, 2014, vol. 139, pp. 5765–71.
4. S.J. Dillon and G.S. Rohrer: *J. Am. Ceram. Soc.*, 2009, vol. 92, pp. 1580–85.
5. H. Beladi, N.T. Nuhfer, and G.S. Rohrer: *Acta Mater.*, 2014, vol. 70, pp. 281–89.
6. G.B. Hardy and D.P. Field: *Metall. Mater. Trans. A*, 2015, vol. 46A, pp. 2273–84.
7. J. Pospiech, K. Sztwiertnia, and F. Haessner: *Texture Microstruct.*, 1986, vol. 6, pp. 201–15.
8. D.M. Saylor, A. Morawiec, and G.S. Rohrer: *Acta Mater.*, 2003, vol. 51, pp. 3663–74.
9. K. Glowinski and A. Morawiec: *Metall. Mater. Trans. A*, 2014, vol. 45A, pp. 3189–94.
10. D.P. Field and B.L. Adams: *Acta Metall. Mater.*, 1992, vol. 40, pp. 1145–57.
11. H.G. Jones, K.P. Mingard, and D.C. Cox: *Ultramicroscopy*, 2014, vol. 139, pp. 20–28.
12. http://mimp.materials.cmu.edu/~gr20/Grain_Boundary_Data_Archive/.
13. M.A. Groeber and M.A. Jackson: *Integr. Mater. Manuf. Innov.*, 2014, vol. 3, p. 5.
14. K. Glowinski: *Methods for Quantitative Characterization of Three-Dimensional Grain Boundary Networks in Polycrystalline Materials*, Institute of Metallurgy and Materials Science, Polish Academy of Sciences, Krakow, 2015.
15. C. Bradford Barber, D.P. Dobkin, and H. Huhdanpaa: *ACM Trans. Math. Softw.*, 1996, vol. 22, pp. 469–83.
16. A. Thorvaldsen: *Mater. Sci. Forum*, 1992, vols. 94–96, pp. 307–12.
17. R. Quey, P.R. Dawson, and F. Barbe: *Comput. Method Appl. M.*, 2011, vol. 200, pp. 1729–15.